Physics Letters A 379 (2015) 206–210

Contents lists available at ScienceDirect

Physics Letters A

www.elsevier.com/locate/pla

Antiperovskite compounds $SbNSr_3$ and $BiNSr_3$: Potential candidates for thermoelectric renewable energy generators

M. Bilal [a,b], Saifullah [a,b], M. Shafiq [a,b], B. Khan [a,b], H.A. Rahnamaye Aliabad [c], S. Jalali Asadabadi [d], Rashid Ahmad [e], Iftikhar Ahmad [a,b,*,1]

[a] Center for Computational Materials Science, University of Malakand, Chakdara, Pakistan
[b] Department of Physics, University of Malakand, Chakdara, Pakistan
[c] Department of Physics, Hakim Sabzevari University, Sabzevar, Iran
[d] Department of Physics, Faculty of Science, University of Isfahan (UI), 81744 Isfahan, Iran
[e] Department of Chemistry, University of Malakand, Chakdara, Pakistan

ARTICLE INFO

Article history:
Received 25 September 2014
Received in revised form 5 November 2014
Accepted 12 November 2014
Available online 18 November 2014
Communicated by R. Wu

Keywords:
Thermoelectric materials
Alternative energy resources
Seebeck coefficient
Antiperovskites $SbNSr_3$ and $BiNSr_3$

ABSTRACT

This letter communicates thermoelectric properties of antiperovskites $SbNSr_3$ and $BiNSr_3$, using ab-initio calculations. These compounds are identified as good transport materials for their narrow band gaps and dense electronic states near their Fermi levels. The peak values of Seebeck coefficient of 1590 and 1540 μV/K are observed for $SbNSr_3$ and $BiNSr_3$, respectively in the *p*-type regions, at room temperature. The figure of merit approaches unity for both materials, while their thermal conductivities increase and electrical conductivities decrease with temperature. These theoretical studies predict that these antiperovskites could be efficient materials for thermoelectric generators and need further experimental and theoretical studies.

1. Introduction

The demand of energy is growing with the quality of life, increase in human population and depletion of fossil fuels. The solution to the problem is not possible by a single source; therefore, different means of renewable energy are investigated to resolve the energy crisis of the world. Extensive experimental and theoretical studies are in progress in fossil fuel alternatives, one of which is thermoelectricity. Conventionally, thermoelectricity is considered as the most suitable source for waste heat recovery where materials with high figure of merit (ZT) are commonly used in thermoelectric generators for large-scale power generation [1–4].

In the present letter, we explore thermoelectric (TE) properties of antiperovskites $SbNSr_3$ and $BiNSr_3$ because of their narrow band gaps and dense electronic states near Fermi level in both valance and conduction bands. This identifies them to be potential materials for thermoelectric devices and hence good sources of green energy in thermoelectric power generators, devices which directly convert thermal energy into electrical energy. The synthesis of $SbNSr_3$ and $BiNSr_3$ is reported by Gäbler et al. [5] for the first time in 2004. They investigated some of their physical properties, including band gaps using diffuse reflectivity method and obtained optical gaps of 1.15 eV for $SbNSr_3$ and 0.89 eV for $BiNSr_3$. They also calculated the electronic band gaps for these materials within Local Density Approximation (LDA) and obtained very small band gap values arguing that LDA severely underestimates band gaps of crystalline materials. In another theoretical study, Haddadi et al. [6] worked on the electronic properties of these materials using the Generalized Gradient Approximation (GGA). The authors obtained band gaps of 0.31 eV for $SbNSr_3$ and 0.26 eV for $BiNSr_3$, which were later on improved by Hichour et al. [7] using modified version of GGA, i.e. Engel and Vosko GGA (EV-GGA) and achieved band gaps of 0.55 and 0.36 eV for $SbNSr_3$ and $BiNSr_3$, respectively but still severely underestimated results.

Thermoelectric properties are highly sensitive to band gaps, and therefore accurate calculated band gaps are required in the theoretical studies of the thermoelectric materials for their logical and rational results for practical applications. Realizing this important aspect of the thermoelectric compounds, we use a recently developed DFT based theoretical technique, improved modified Becke–Johnson (I-mBJ) potential [8] for high accuracy of the band gaps, while using these electronic structures, the thermoelectric properties of the compounds are explored.

* Corresponding author. Tel.: +92 332 9067866.
E-mail address: ahma5532@gmail.com (I. Ahmad).
[1] Ph.D. (Idaho), Professor of Theoretical Physics, University of Malakand.

http://dx.doi.org/10.1016/j.physleta.2014.11.016
0375-9601/

2. Theory and computational details

The full potential linearized augmented plane waves (FP-LAPW) method, based on density functional approach [9,10] as implemented in the WIEN2k [11] is used to calculate the electronic properties of $SbNSr_3$ and $BiNSr_3$. The experimental lattice constants of $SbNSr_3$ and $BiNSr_3$, i.e. 5.1725 Å and 5.2069 Å respectively [5], are used as input variables to calculate theoretical lattice constants for both materials. The calculated relaxed lattice parameters are used to calculate the electronic properties of the compounds. For achieving accurate band gaps we used improved modified Becke–Johnson (I-mBJ) [8] potential. The modified Becke–Johnson (mBJ) potential [12] is:

$$v_x^{TB\text{-}mBJ}(r) = c\,v_x^{BR}(r) + (3c-2)\frac{1}{\Pi}\sqrt{5/12}\sqrt{2t(r)/\rho(r)} \tag{1}$$

where c is defined as

$$c = A + B\sqrt{\bar{g}} \tag{2}$$

and

$$\bar{g} = \frac{1}{v_{cell}}\int_{cell}\frac{1}{2}\left(\frac{|\nabla\rho^{\uparrow}(r)|}{\rho^{\uparrow}(r)} + \frac{|\nabla\rho^{\downarrow}(r)|}{\rho^{\downarrow}(r)}\right)d^3r \tag{3}$$

where $\bar{g}$ is the average of $g = |\nabla\rho|/\rho$, while ρ is the electronic density. The values of A and B in Eq. (2) are taken as -0.012 and $1.023\ (\text{Bohr})^{1/2}$, respectively in the mBJ potential [12]. Koller et al. [8] introduced new values of $A = 0.488$ and $B = 0.500\ (\text{Bohr})^{1/2}$ for large band gap materials and $A = 0.267$ and $B = 0.656\ (\text{Bohr})^{1/2}$ for small band gap materials, by minimizing mean-absolute relative error (MARE) of few solids, and hence modified Eq. (2) as follows:

$$c = A + B\bar{g}^{e} \tag{4}$$

where $e = 1$ for simplicity. In the present work, we use $A = 0.267$ and $B = 0.656\ (\text{Bohr})^{1/2}$ as both $SbNSr_3$ and $BiNSr_3$ are small band gap materials. For $SbNSr_3$ the calculated values of $c = 1.2016$ and $g = 1.4247$, while for $BiNSr_3$ $c = 1.1913$ and $g = 1.4067$. Between the core and valence states, the separation energy in this work is kept at -6.0 Ry. In the full potential scheme the wave functions inside the atomic spheres for both materials are expanded in terms of spherical harmonics up to $l_{max} = 10$. The convergence parameter $R_{MT}K_{max}$, is set to 7 and R_{MT}'s are fixed as 2.5 (Sb), 2.22 (N) and 2.33 (Sr) Bohr for $SbNSr_3$ and 2.5 (Bi), 2.41 (N) and 2.5 (Sr) Bohr for $BiNSr_3$. The plane wave cut off value for the charge density and potential is selected to be $G_{Max} = 12\ (\text{Ry})^{1/2}$. 500 k-points are used for electronic properties calculations.

The calculated electronic structures are further used to calculate thermoelectric properties of $SbNSr_3$ and $BiNSr_3$ materials, like Seebeck coefficients, thermal conductivities and electrical conductivities, using BoltzTraP [13] code. The transport coefficients based on the rigid band approach to conductivity are explained by using Eq. (1) as given below:

$$\sigma_{\alpha\beta}(\varepsilon) = \frac{1}{N}\sum_{i,k}\sigma_{\alpha\beta}(i,k)\frac{\delta(\varepsilon-\varepsilon_{i,k})}{\delta(\varepsilon)} \tag{5}$$

$$\sigma_{\alpha\beta}(i,\vec{k}) = e^2\tau_{i,k}v_{\alpha}(i,\vec{k})v_{\beta}(i,\vec{k}) \tag{6}$$

where, N is the number of k-points. Eq. (6) explains k-dependent transport tensors, where τ is the relaxation time, and $v_{\alpha}(i,\vec{k})$ is a component of group velocity. The transport coefficients, which are the function of temperature (T) and chemical potential (μ), i.e. electrical conductivity and Seebeck coefficient tensors can be found by integrating the transport distribution [13,14]:

$$\sigma_{\alpha\beta}(T,\mu) = \frac{1}{\Omega}\int\sigma_{\alpha\beta}(\varepsilon)\left[-\frac{\partial f_0(T,\varepsilon,\mu)}{\partial\varepsilon}\right]d\varepsilon \tag{7}$$

$$S_{\alpha\beta}(T,\mu) = \frac{1}{eT\Omega\sigma_{\alpha\beta}(T,\mu)} \times\int\sigma_{\alpha\beta}(\varepsilon)(\varepsilon-\mu)\left[-\frac{\partial f_0(T,\varepsilon,\mu)}{\partial\varepsilon}\right]d\varepsilon \tag{8}$$

where, α and β are the tensor indices, e is the electron charge, Ω is the volume of the unit cell, μ is the carrier concentration and f_0 is the Fermi–Dirac distribution function. The relaxation time, τ, is taken constant in this study. The Seebeck coefficient is calculated by the band structure calculation as it does not depend on relaxation time but electrical conductivity needs to be calculated with respect to the relaxation time.

3. Results and discussion

Thermoelectric properties are sensitive to electronic properties and therefore accurate band gap value of a material is required for its reliable thermoelectric nature. The band structures of $SbNSr_3$ and $BiNSr_3$ are calculated by the I-mBJ [8] potential and are presented in Fig. 1. The overall band profiles of these compounds are in good agreement with the previous theoretical works [6,7], where the top of the valance bands and bottom of the conduction bands lie at Γ point for both materials, resulting in direct band gap semiconductors. Unlike the other theoretical works the band gaps obtained by the I-mBJ for $SbNSr_3$ and $BiNSr_3$ are consistent with the experimental values. Table 1 clearly indicates that I-mBJ is very effective in the prediction of band gaps of these compounds and also confirms the superiority of this theoretical method over LDA [5], GGA [6], and EV-GGA [7]. The accurate I-mBJ electronic structures of $SbNSr_3$ and $BiNSr_3$, as shown in Fig. 1, are further used to calculate the thermoelectric properties of these compounds.

The greatest challenge in thermoelectric power generators is to find highly efficient TE materials. The efficiency of a TE material depends on its stringent physical properties [15,16]. One of the main requirements for a good TE material is its figure of merit, $ZT = \sigma S^2 T/k$, where it is directly related to Seebeck coefficient (S) of that material. Therefore, compounds with high S are considered to be good TE materials [17,18]. In Seebeck effect, the temperature difference across the ends of a thermoelectric material causes potential difference, which pushes electrons from one end to the other.

In Fig. 2(a)–(b), Seebeck coefficients for $SbNSr_3$ and $BiNSr_3$ are presented at different temperatures, 300, 600 and 900 K. It is clear from the plots that the response of the materials is the same in both p-type and n-type regions. In the p-type region, $SbNSr_3$ shows the peak value of 1590 μV/K, while $BiNSr_3$ shows the peak value of 1540 μV/K at room temperature, which predict that these are good TE materials. Similarly, both materials show good response in n-type region too. The plots show that the Seebeck coefficient decreases exponentially with temperature. Furthermore, it can be seen that the Seebeck coefficient exists between -0.3 μ(eV) and 0.3 μ(eV) of the chemical potential and becomes zero beyond these points. Hence, materials are strongly responsive in this region. The comprehensive study of the plots reveals that both of the materials show approximately the same behavior with small differences in details.

Thermal conductivity is the flow of heat in a material for which electrons and lattice vibrations are responsible. In TE devices, materials having small thermal conductivity are used so that the temperature difference may not be disturbed. Fig. 3(a)–(b) presents the electronic thermal conductivities for $SbNSr_3$ and $BiNSr_3$ at 300, 600 and 900 K. It is clear from the figure that thermal conductivities increase with the increase in temperature; which is obvious as

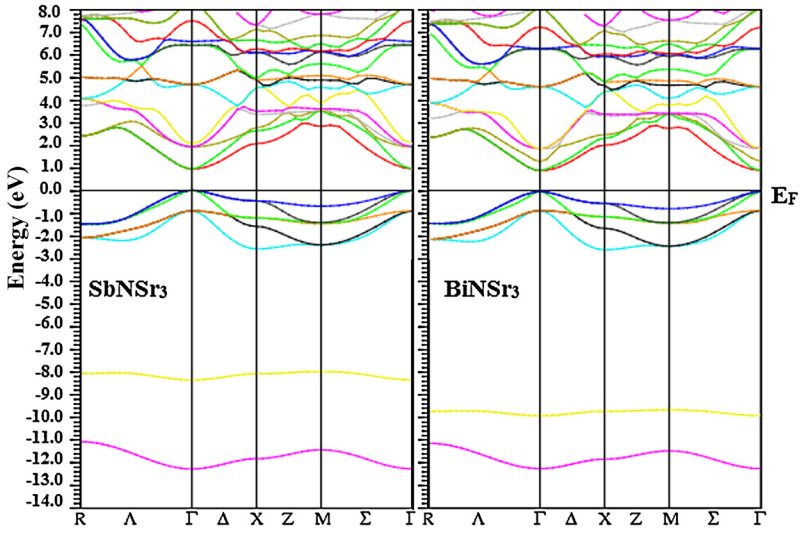

Fig. 1. Band structures for $SbNSr_3$ and $BiNSr_3$ by improved modified Becke–Johnson potential (I-mBJ).

Table 1
Calculated band gaps (in eV) for $SbNSr_3$ and $BiNSr_3$ are compared with the experimental and other theoretical results.

	Present work	Exp. work	Other work		
	I-mBJ		EV-GGA	GGA	LDA
$SbNSr_3$	0.92	1.15[a]	0.55[c]	0.31[b]	0.15[a]
$BiNSr_3$	0.81	0.89[a]	0.36[c]	0.26[b]	0.15[a]

[a] Exp. [5].
[b] [6].
[c] [7].

the energy of free electrons increase with temperature. The figure shows that both materials have approximately the same behavior. Thermal conductivities remain zero at room temperature between −0.3 μ(eV) and 0.3 μ(eV) of the chemical potential, so high figure of merit can be attained in this region. The plots reveal that the thermal conductivities are smaller in the *p*-type region as compared to the *n*-type region for both materials.

The flow of free electrons in a material is termed as electrical conductivity. Electrons gain energy with temperature and move from high temperature regions to the low temperature regions. This movement of electrons in a TE material causes electric current. For good TE properties, materials should have high values of electrical conductivity. The electrical conductivities for $SbNSr_3$ and $BiNSr_3$ at different temperatures, i.e. 300, 600 and 900 K, are presented in Fig. 4(a) and (b), respectively. The response of electrical conductivities for both materials is approximately the same at a given temperature. The threshold points for the electrical conductivities of these materials in *p*-type and *n*-type regions are −0.25 μ(eV) and 0.25 μ(eV) chemical potentials, respectively. Electrical conductivities remain zero between these points while beyond these points materials have good electrical conductivities and at the 1.4 μ(eV) chemical potential we get the peak values of $5.7 \times 10^{20}/\Omega\,\mathrm{m\,s}$ and $5.6 \times 10^{20}/\Omega\,\mathrm{m\,s}$ for *n*-type $SbNSr_3$ and $BiNSr_3$, respectively. Chemical potential is regarded as carrier density [19] therefore, in the vicinity of zero chemical potential, carrier density will be small. Due to this small carrier density, there will be minimum conduction charges available, resulting in low values of electrical conductivities near zero chemical potential. As conduction charges are responsible for electronic thermal conductivity, the unavailability of carriers in this region is also the cause of minimum electronic thermal conductivity.

The performance of any device is important issue, while in a thermoelectric device the efficiency can be measured by the figure

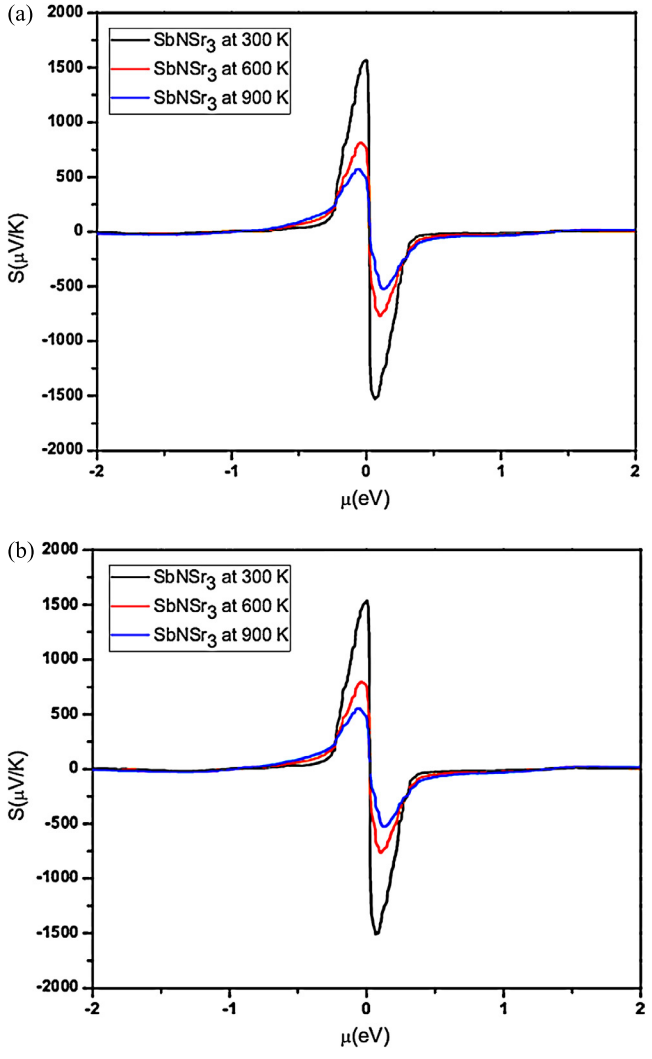

Fig. 2. Seebeck coefficients for (a) $SbNSr_3$ and (b) $BiNSr_3$ as a function of chemical potential at 300, 600 and 900 K.

of merit of the TE material. The figure of merit of a TE material is represented by ZT, which mathematically is given by:

$$ZT = \sigma S^2 T/\kappa \tag{9}$$

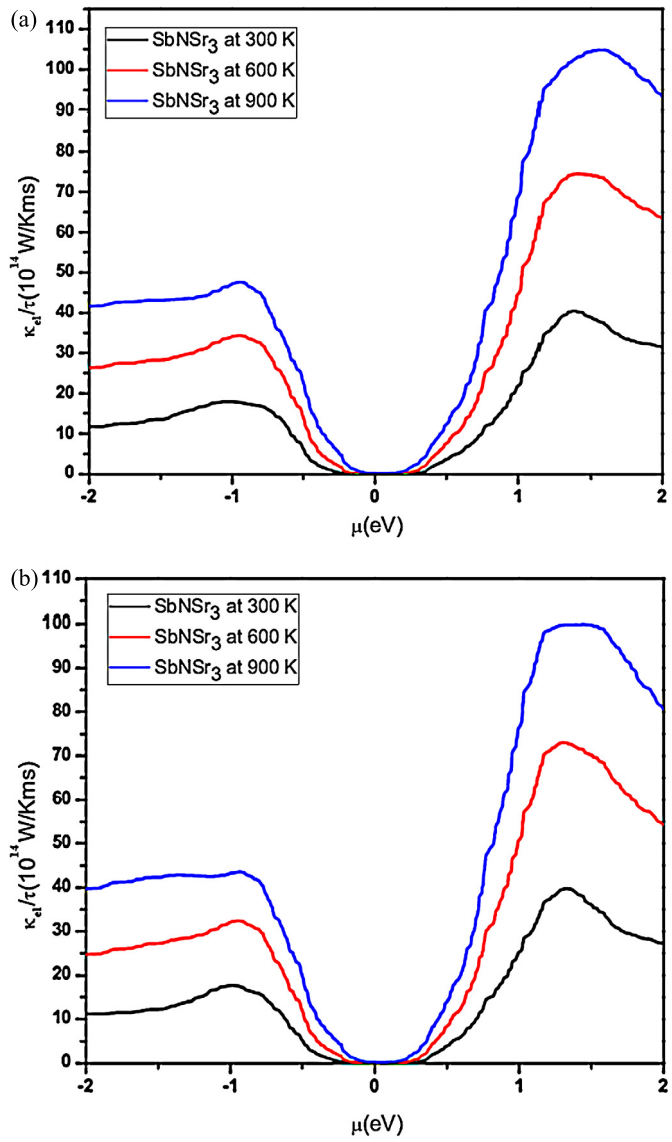

Fig. 3. Electronic thermal conductivities for (a) $SbNSr_3$ and (b) $BiNSr_3$ as a function of chemical Potential at 300, 600 and 900 K.

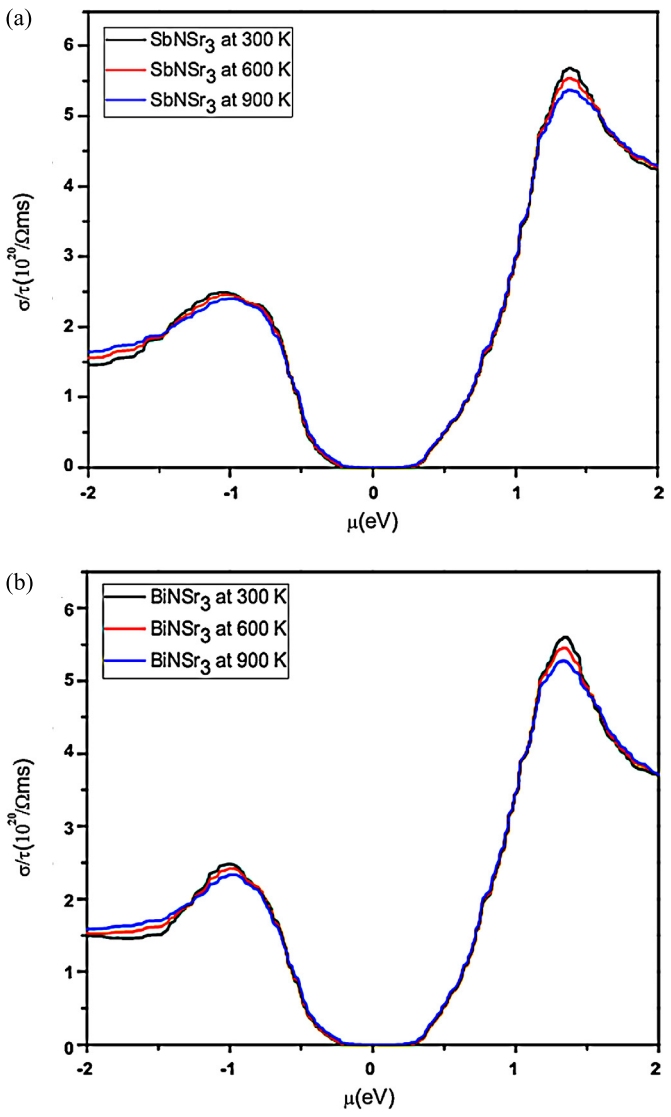

Fig. 4. Electrical conductivities for (a) $SbNSr_3$ and (b) $BiNSr_3$ as a function of chemical potential at 300, 600 and 900 K.

where S represents the Seebeck coefficient, σ represents the electrical conductivity and k represents thermal conductivity. It is clear from the equation that the figure of merit is directly proportional to S^2 and electrical conductivity, whereas it is inversely proportional to the thermal conductivity. Therefore, if S^2 and electrical conductivity are larger and thermal conductivity is smaller, then the figure of merit will be larger. The Seebeck coefficient, as presented in Fig. 2, gives maximum values between -0.3 and 0.3 μ(eV) chemical potential whereas, is zero at Fermi level (middle of band gap) because there are no electrons and holes in the Fermi level. Therefore, S^2 is zero at Fermi level. The thermoelectric values are positive when the Fermi level shifts down towards the valence band indicating p-type conduction and the Seebeck coefficients are negative when the Fermi level shifts upward to the conduction band indicating n-type conduction. Consequently, for bottom and top of Fermi level there are two maximum and minimum for the Seebeck coefficients. This is true that between -0.3 and 0.3 μ(eV) chemical potential, the electrical conductivity is almost zero and has nonzero values only at the border of this interval, but we should notice that the electronic thermal conductivity is also very small inside this interval. Therefore, due to high values of Seebeck coefficient and low values of electronic thermal conductivity in this region, we expect maximum thermoelectric response. This expectation is in excellent agreement with our calculated ZT, as shown in Fig. 5.

Materials having ZT around unity exhibit good thermoelectric properties [20,21] and can be used for electric power generation in TE devices. Fig. 5(a)–(b) shows the graphs of the figure of merit against chemical potential for $SbNSr_3$ and $BiNSr_3$, at temperatures 300, 600 and 900 K, respectively. It is clear from the figures that both materials show approximately the same behavior with the figure of merit approaching unity. At room temperature the figures of merit for both materials are about 0.99, which identifies them as good candidates for TE devices. For $SbNSr_3$, ZT sharply rises as chemical potential increases from zero in both n-type and p-type regions and we get the peaks at 0.2 μ(eV) and -0.2 μ(eV). Then it drops to zero at 0.6 μ(eV) and -0.6 μ(eV). We get maximum output around 0.2 and -0.2 μ(eV) because Seebeck coefficient is maximum and thermal conductivity is minimum in these regions. Furthermore, ZT approach zero beyond 0.6 and -0.6 μ(eV) because Seebeck coefficient is zero and thermal conductivity is larger beyond these points. We see small values of ZT in this region for the reason that electrical conductivity gives peak values beyond -0.3 and 0.3 μ(eV).

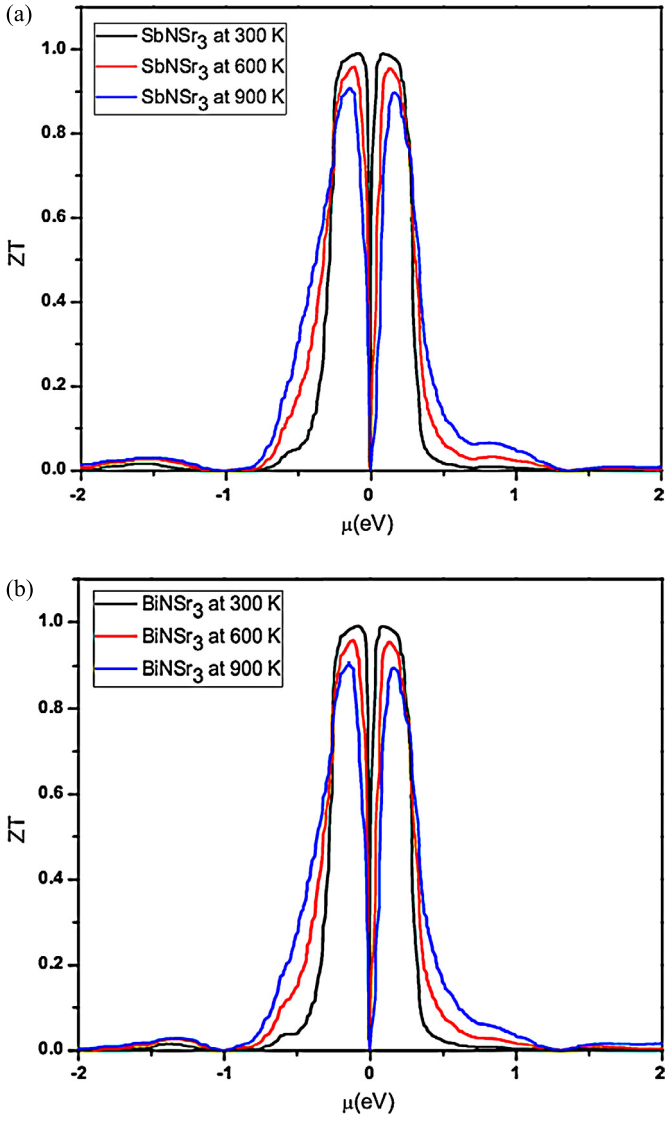

Fig. 5. Graphs of ZT vs. chemical potential for (a) $SbNSr_3$ and (b) $BiNSr_3$ at 300, 600 and 900 K.

4. Conclusions

In conclusion, we studied band structures of $SbNSr_3$ and $BiNSr_3$ using improved modified Becke–Johnson potential and got closer band gap values to the experimental than the previous theoretical results. The thermoelectric properties of these compounds are calculated and very interesting and promising results are obtained for these materials at room temperature. The figure of merit for these materials approaches unity which reveals that these materials can be useful in thermoelectric power generators. High values of Seebeck coefficients are obtained between −0.3 and 0.3 μ(eV) chemical potential, while their thermal conductivities are zero in this region. Therefore, peak values for the figure of merit are obtained in this region. Maximum values for electrical conductivities are obtained beyond −0.5 and 0.5 μ(eV) of the chemical potential in the *p*-type and *n*-type region, respectively. For this reason, small values of the figure of merit beyond these points are observed. The overall patterns of the figure of merit clearly show that $SbNSr_3$ and $BiNSr_3$ are good thermoelectric materials and can be efficiently used in thermoelectric power generators as an alternative green energy sources.

References

[1] L.E. Bell, Science 321 (2008) 1457.
[2] D. Kraemer, B. Poudel, H.P. Feng, J.C. Caylor, B. Yu, X. Yan, Y. Ma, X. Wang, D. Wang, A. Muto, K. McEnaney, M. Chiesa, Z. Ren, G. Chen, Nat. Mater. 10 (2011) 532.
[3] Y. Pei, X. Shi, A.L. Londe, H. Wang, L. Chen, Nature 473 (2011) 66.
[4] D.S. Dalafave, Mater. Chem. Phys. 119 (2010) 195.
[5] F. Gäbler, M. Kirchner, W. Schnelle, U. Schwarz, M. Schmitt, H. Rosner, R. Niewa, Z. Anorg. Allg. Chem. 630 (2004) 2292.
[6] K. Haddadi, A. Bouhemadou, L. Louail, F. Rahal, S. Maabed, Comput. Mater. Sci. 46 (2009) 881.
[7] M. Hichour, R. Khenata, D. Rached, M. Hachemaoui, A. Bouhemadou, A.H. Reshak, F. Semari, Physica B 405 (2010) 1894.
[8] D. Koller, F. Tran, P. Blaha, Phys. Rev. B 85 (2012) 155109.
[9] O.K. Andersen, Phys. Rev. B 12 (1975) 3060.
[10] W. Kohn, L. Sham, Phys. Rev. 140 (1965) A1133.
[11] P. Blaha, K. Schwarz, G.K.H. Madsen, D. Kvasnicka, J. Luitz, Wien2k, an augmented plane wave plus local orbital program for calculating the crystal properties, TU Vienna, Austria, 2001.
[12] F. Tran, P. Blaha, Phys. Rev. Lett. 102 (2009) 226401.
[13] G.K.H. Madsen, D.J. Singh, Comput. Phys. Commun. 175 (2006) 67.
[14] T.J. Scheidemantel, C. Ambrosch-Draxl, T. Thonhauser, J.V. Badding, J.O. Sofo, Phys. Rev. B 68 (2003) 125210.
[15] P. Ruleovaa, C. Drasar, P. Lostak, C.P. Li, S. Ballikaya, C. Uher, Mater. Chem. Phys. 119 (2010) 299.
[16] X. Qu, W. Wang, W. Liu, Z. Yang, X. Duan, D. Jia, Mater. Chem. Phys. 129 (2011) 331.
[17] S. Peng, H. Kawanamic, Y.K. Li, G.H. Li, Q. Huang, J.M. Zhou, J. Cryst. Growth 227 (2001) 786.
[18] D.C. Grauer, Y.S. Hor, A.J. Williams, R.J. Cava, Mater. Res. Bull. 44 (2009) 1926.
[19] V. Ugarte, V. Aji, C.M. Varma, Phys. Rev. B 84 (2011) 165429.
[20] O. Rabin, L. Yu-Ming, M.S. Dresselhaus, Appl. Phys. Lett. 79 (2001) 81.
[21] T. Takeuchi, Mater. Trans. 50 (2009) 2359.